Preheating and Premixing Effects on NO_x Emissions in a High-Pressure Axially Staged Combustor

Tommy Genova, Jr.[1], Michelle Otero[1], Anthony Morales[1], Bernhard Stiehl[1], Scott Martin[2], Kareem Ahmed[1*]

[1]Center for Advanced Turbomachinery and Energy Research, Department of Mechanical and Aerospace Engineering, University of Central Florida, Orlando, FL, 32816, United States

[2]Embry-Riddle Aeronautical University, Daytona Beach, FL, 32114, United States

*Corresponding author. Email Address: Kareem.ahmed@ucf.edu

Abstract

NO_x emissions remain a primary concern for modern and future gas turbines, particularly as we progress towards a net-zero carbon future. It is critical to identify novel strategies to mitigate environmental pollutants for both modern turbines operated on natural gas and future turbines projected to use carbon-free fuels (such as hydrogen). In the current study, NO_x emissions of a reacting methane-air jet in a vitiated crossflow are experimentally investigated in a model axially staged combustor at 5 atm. The combustion products from the main stage combustor flow into the axial stage at temperatures ranging from 1580-1650°C. The axial stage contains a reacting jet in crossflow which provides an overall temperature rise ranging from 50-220°C to generate exit temperatures similar to gas turbine engines. The focus of this paper is to explore the effects of flame liftoff and ignition timescales on the NO_x contribution of this secondary jet. This is done by varying the premixed level and preheat temperature of the axial jet. The effects are explored at different momentum flux ratios (J), jet equivalence ratios (φ_{jet}), exit temperatures (T_{exit}), and main stage (headend) temperatures (T_{HE}). High-speed CH*

chemiluminescence imaging is employed for each test case to determine the flame stabilization point. For a given temperature rise and combustor exit temperature, an increase in ignition delay was observed with a decrease in jet temperature. This provided a NO_x benefit, particularly for jets that are injected at or close to an ignitable mixture fraction. Similarly, the coaxial injector caused a significant ignition delay compared to the fully premixed injector; this also led to a NO_x benefit. Overall, the results show that a thermally driven delay in the axial stage provides a greater NO_x reduction than a mixing delay.

1. Introduction

As society trends towards a zero-carbon future, pollutant emissions will remain a concern for gas turbine-based power generation. In current natural gas-powered turbines, NO_x emissions are the main design constraint limiting turbine efficiency. Future, zero-carbon gas turbines are also projected to be limited on NO_x emissions as NO_x is the only major pollutant present in hydrogen-air combustion. Initiatives to mitigate NO_x have been underway in recent years. For gas turbines, dry low NO_x (DLN) combustors have reduced NO_x output by running lean premixed flames to mitigate local hot regions [1-5]. This has allowed for increased turbine inlet temperatures which correspond to improved turbine efficiency. To further increase turbine firing temperature and reduce NO_x, axially staged combustion strategies have been implemented in modern turbines. Axially staged combustion is a combustion technique that splits the combustion process into separate stages. The main (headend) stage is fully premixed and burned at a lean equivalence ratio while the secondary (axial) stage consists of a reacting jet-in-crossflow injected downstream into the products of the main stage. The secondary fuel injection generates an

overall temperature rise near the turbine inlet which reduces the residence time the products spend at a higher temperature. This effectively reduces NO_x as the formation of NO_x is directly coupled with residence time [6]. Because the amount of fuel burnt in the axial stage can be varied, this technique has proven to also work at lower loading conditions where CO burnout to CO_2 is critical. One of the challenges of axially staged combustion is careful tuning of the residence time is required for each operating condition to ensure complete combustion in the axial stage. Additionally, having multiple flow paths adds design complexities. Hence, additional research is beneficial to improve axial stage technologies.

The flame-flow field interaction is critical in the axial stage as the turbulent mixing and entrainment processes have a strong influence on flame stabilization and NO_x production. Recent work done at the University of Connecticut characterized flame stability in an atmospheric facility; the windward flame branch exhibited an instability where the stabilization point went from fully attached to completely blown off while the leeward flame branch remained attached to the jet exit [7-9]. Similar flow-field and wake characteristics were investigated at the University of Cincinnati and Li et al. using circular and slotted jet geometries at atmospheric pressure [10-13]. These flow-field features have a strong influence on flame stabilization which ultimately affects NO_x production.

For gas turbine flames, NO_x forms mainly through two different paths: the prompt NO and thermal NO pathways. NO_x formation at temperatures hotter than 1800 K is dominated by the thermal NO pathway also known as the Zel'dovich NO mechanism. Because the activation energy required to break the triple bond of N_2 is high, the thermal NO reaction is only fast at high temperature and is found primarily in the post-flame gases [14]. As a result of this, residence

time (τ_{res}) and local hot regions are the main sources of NO formation in gas turbine combustors. Localized hot regions are driven by rich mixture fractions at the flame location caused mainly by poor mixing.

NO_x emissions of partially premixed flames have been widely documented [15-19]. Gore and Zhan investigated NO_x emissions of partially premixed rich methane-air flames where air was injected coaxially around the fuel stream. As the burner equivalence ratio was increased passed stoichiometric conditions, NO_x emissions decreased until an optimum point was reached between $1.9 \leq \varphi \leq 2.1$ and then increased when $\varphi \geq 2.1$ [15].

Pre-flame mixing of the jet and crossflow in the axial stage has been shown to have a major influence on NO_x abatement. Consequentially, the flame liftoff of the reacting jet-in-crossflow is critical to NO_x formation. Kolb et al. studied the effects of momentum flux ratio and jet preheat temperature on flame liftoff [20]. For lean jets, increasing the equivalence ratio decreased liftoff, while increasing jet preheat temperature had little effect on liftoff. Sirignano et al. explored the coupling between liftoff and NO_x emissions in an atmospheric pressure facility by increasing jet equivalence ratio for a given temperature rise [21, 22]. For a constant temperature rise, an increase in liftoff provided a NO_x benefit. This was attributed to the enhanced pre-flame mixing of the jet and crossflow with increasing liftoff. Liftoff and stabilization were dependent on equivalence ratio and momentum flux ratio; NO_x for leeward stabilized flames were found to be particularly sensitive to liftoff. This trend was also observed by Ahrens et al. who investigated NO_x formation in a swirl stabilized atmospheric pressure facility [23]. A numerical model generated based on the experimental data considered the best-case scenario: perfect mixing of the jet and crossflow before ignition, and the worst-case scenario: no mixing of

the jet and crossflow prior to ignition. The numerical model showed the effect of pre-flame mixing on NO_x reduction to be stronger at atmospheric conditions. Goh et al. used a chemical reactor network to predict the minimum achievable NO_x with fuel staging [24]. 1 ppm NO_x was determined to be theoretically achievable for gas turbine conditions. However, this theoretical limit does not account for the coupling of the chemical kinetics and fluid mechanics in the axial stage.

Because gas turbines are operated at high pressure, data at elevated pressure is of interest to industry. Studies at elevated pressure include Panda et al. who studied a reacting jet stabilized in a swirl crossflow at 5.5 atm [25-28]. Sullivan et al. investigated a fuel jet consisting of blends of CH_4/H_2 at 6 atm [29]. NO_x emissions were found to increase linearly with temperature rise across the axial stage independent of jet composition. Lamont et al. and Roa et al. studied NO_x emissions of different jet injectors at various equivalence ratios in a 5.5 atm low-swirl crossflow facility; compared to the single-stage combustor, staging benefits were observed for lean-near stoichiometric equivalence ratio jets at low momentum flux ratios [30, 31]. Prathap et al. investigated NO_x formation in an axially staged combustion system at elevated pressures of 5-8 atm [32]. NO_x formation was not sensitive to the jet injection velocity; additionally, at higher pressure, the flame was located closer to the injector. A recent investigation by Rodrigues et al. explored the effects of combustor exit Mach number on NO_x emissions in high-subsonic flow [33]. For a constant residence time, an increase in combustor exit Mach number provided a reduction in NO_x. This was attributed to lower static temperatures and improved mixing with increased Mach number.

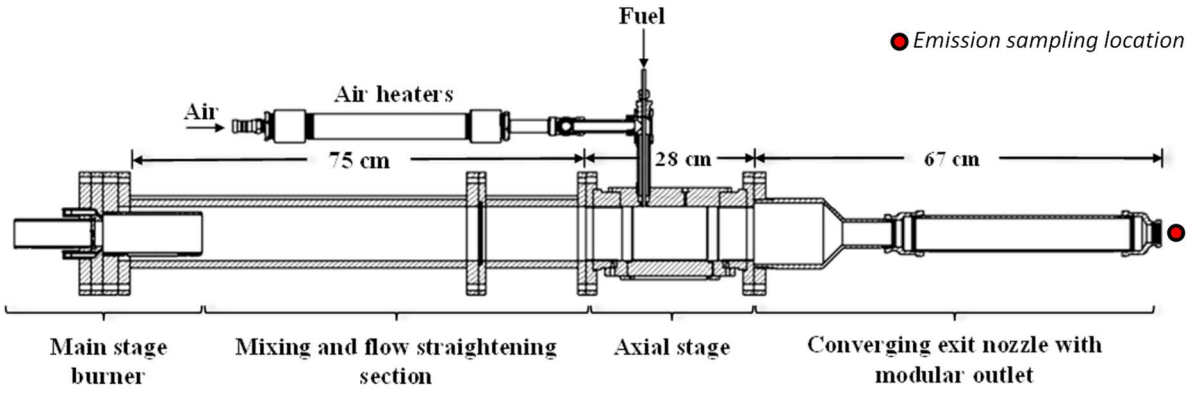

Fig. 1. Overview of 5 atm experimental facility

The goal of the current study is to expand upon recent experimental work and characterize the effects of jet preheat temperature and level of premixing between the fuel and air on NO_x emissions and flame characteristics in the axial stage of a model gas turbine combustor. The research is conducted in an axially staged combustion facility at elevated pressure that has been tuned to produce conditions relevant to ground-based power generating gas turbines. High-speed CH* chemiluminescence is employed to determine the flame stabilization point. The analysis is focused on the effects of flame liftoff and ignition timescales for NO_x mitigation at various engine-relevant conditions. The variation in jet temperature provides a thermally driven delay while a non-premixed configuration alters the jet mixing. For both configurations, a NO_x reduction was strongly coupled to an increase in ignition timescale; delaying ignition through a thermal mechanism was determined to have more of an effect on NO_x reduction than delaying ignition through a non-premixed configuration.

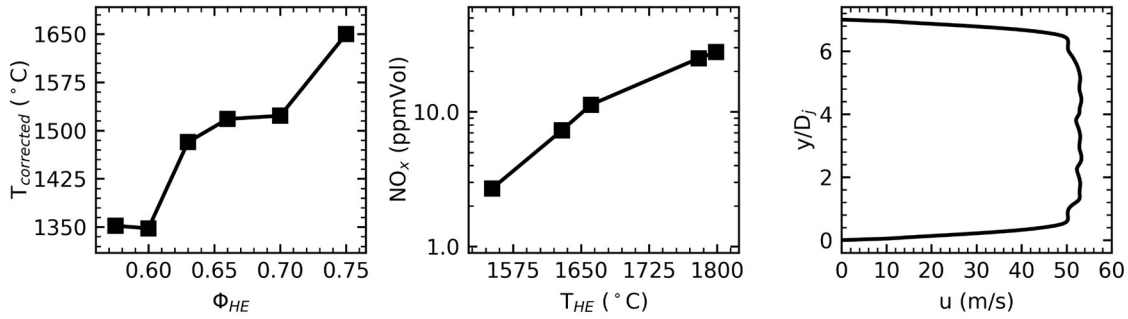

Fig. 2. Temperature, velocity, and NO_x calibration at inlet of test section

2. Experimental Methods

2.1 Experimental Facility

The experimental facility is divided into three sections: the main stage burner, the axial stage (test section), and the contoured exit nozzle that can be varied in area and length. Flow to the facility is controlled by solenoid valves for the fuel lines and actuated valves for the airlines. The fuel lines are metered using O'Keefe precision orifices, and the airlines are individually metered using USA Industry restriction orifice unions (ROUs). The discharge coefficient for each union was calibrated using a Coriolis flowmeter and is accurate within 2%. Upstream of the unions are Dwyer pressure transmitters used to measure the pressure of the incoming flow. This is used along with the discharge coefficient to modulate the mass flow rate based on the choked flow at the orifice. The uncertainty associated with the equivalence ratios is $\pm$ .04 and comes from the error propagation relating to the pressure measurements that are used to measure the mass flow rates. A National Instruments (NI) DAQ is used to control the timing of each valve and record pressure and temperature measurements. At the exit of the facility, the flow is choked creating a back pressure based on the mass flow rate. By adjusting the exit area, the Reynolds number of the facility can be adjusted for a given pressure. For the current work, the pressure was held

constant at 5 atm, but the facility can run as high as 10 atm. A schematic of the test facility is provided in Fig. 1.

In the main stage burner, a fully premixed methane/air mixture is ignited in the recirculation region generated between the injector pipe and the large inner pipe inside the facility. Hydrogen is injected at a 45° angle into the recirculation zone for improved stability; hydrogen makes up less than 3% of the total fuel in the main burner stage. Additional air is injected coaxially around the main burner pipe to decrease the overall equivalence ratio of the main stage and cool the combustor walls. For the current study, it was found that splitting too much main stage air to the coaxial lines leads to increased equivalence ratios in the main burner pipe which caused significant NO_x formation. As a result of this, only 5-7% of the overall main stage air was split to the coaxial lines to keep NO_x formation in the main stage low.

The products of the main stage flame exit the central burner pipe into the 76x89 mm plenum where they mix with the additional air. The vitiated flow passes through a 76 cm mixing section which contains a 40% open area perforated screen 23 cm upstream of the test section. The perforated screen creates a top-hat velocity profile for the axial stage to prevent crossflow irregularities from interfering with the axial stage measurements. Previous work has quantified velocity profiles through particle image velocimetry (PIV) and temperature measurements at the inlet of the axial stage [34]. Fig. 2 shows the temperature, velocity, and NO_x curves at the inlet of the test section. Temperature measurements were made at the center point at the inlet of the test section using an exposed bead b-type thermocouple, and a correction factor for radiation was applied. Measurements at the centerline were found to be in close agreement with adiabatic flame temperatures. NO_x measurements made at the inlet of the test section were found to be

minimal below 1600°C. A sample velocity profile at the inlet of the test section made from PIV is also shown. For the current study, the main stage is operated between 1580-1650°C and 49-55 m/s. This corresponds to Reynolds numbers between 200,000-250,000. Note, because the cross-sectional area of the experimental facility is an order of magnitude smaller than actual gas turbines, the Reynolds number is expected to be an order of magnitude smaller. However, the overall trends are expected to hold.

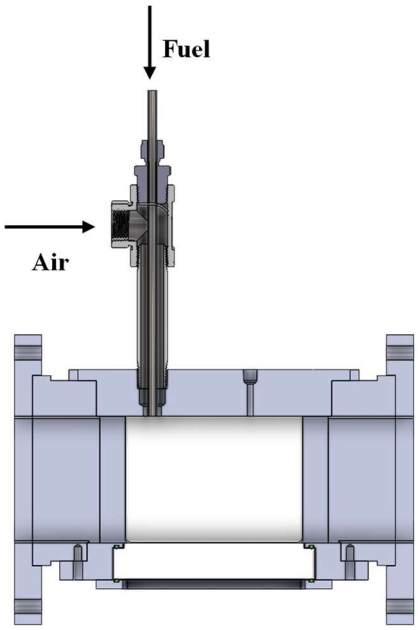

Fig. 1. Test section with non-premixed axial jet configuration

The test section contains three optical viewing windows (two on the side and one on the bottom), and a modular injector top plate. For the current study, a 12.7 mm wall flush-mounted injector was used. Air for the axial stage is passed through two 6,000 W air heaters. Each heater has a thermocouple just downstream of the exit that is connected to a PID controller; the uncertainty associated with the k-type thermocouple was ± 2.2°C. The PID controller controls a relay that cycles on and off the 220 V power source of the heaters at 5 Hz based on the reading from the thermocouple. Air is run through the axial heaters, and when the axial temperature reaches a steady state, the facility is run, and data is collected. Fuel for the axial stage is introduced in two different configurations: fully premixed and non-premixed. For the fully premixed configuration, fuel is introduced to the air 15 jet diameters upstream of the injection point. The fuel-air mixture is passed through a perforated screen that aids in mixing and mitigates pressure oscillations from propagating up the jet injector. For the non-premixed configuration,

fuel is introduced through a 9.5 mm bore-through Swagelok tube that sits flush with the combustor wall as shown in Fig. 3. In this configuration, air is injected into the facility coaxially around the fuel. This creates two mixing streams: the jet with the vitiated crossflow, and the fuel/air mixing of the jet itself. A pressure tap 5.9 cm downstream of the injection point is used to measure the pressure inside the test section.

A flange that adapts the rectangular cross-section to a circular cross-section is located 18.2 cm downstream of the injector. The circular pipe is 102.4 mm in diameter and has a contoured converging section with an NPT fitting on the end. This fitting is connected to a pipe that can be adjusted in length to change the residence time. The exit length for the present investigation was chosen based on initial testing to make certain CO levels were below 20 ppmVol indicating sufficiently complete combustion. At the end of the exit section is another converging section with a 33.4 mm diameter exit. Here the flow is choked, and the facility is pressurized based on the mass flow rate and gas properties of the combustion products. Initial testing of the facility determined the discharge coefficients over the facility's operating range.

2.2 Emissions Sampling and Flame Imaging

A copper emissions probe with a diameter of 21 mm is placed at the exit plane of the facility to capture the exhaust gases. The copper probe is immediately brought to a large ice bath to quench additional NO_x formation. While ice water is used to cool the exhaust gases through the copper probe, the water is never introduced to the combustion products. This ensures accurate measurement without the complication of condensing out the water used for quenching. The exhaust gases are sampled with an E-instruments E4500 emissions analyzer for

300s. The analyzer is equipped with NO low, NO_2 low, CO low, CO_2, and O_2 sensors to obtain accurate measurements of true NO_x (NO + NO_2) and CO. The uncertainty for each NO_x measurement is $\pm$ 0.8 ppmVol corrected to 15% O_2 and the standard deviation for each test point's 300 samples ranged between 0.2-0.5 ppmVol which are used as the error bars. The NO_x emissions measurements are presented as $\Delta NO_x/NO_{x,HE}$ where ΔNO_x is the measured outlet NO_x minus the headend NO_x; this enables the study of the axial jet contribution. The emissions probe was moved around the exit plane for various cases and the change in NO_x levels was on the order of the uncertainty of the analyzer; this indicates the 21 mm probe placed at the center of the 33 mm exit diameter captures an adequate amount of exhaust products to obtain a true global average.

High-speed CH* chemiluminescence was obtained for each test condition to track the flame stabilization point and find the flame liftoff. A Photron SA1.1 with a 50 mm *f/1.2* lens and a 430 nm filter collected images at 20 kHz at a resolution of 512x512. The camera was mounted perpendicularly to the side window of the test section, with a field of view of 89x89 mm; this corresponds to a pixel resolution of 174 μm/pix. For each image, the Otsu method was utilized to determine a non-arbitrary threshold for the flame boundary [35]. Flame liftoff is of particular interest to the current investigation as pre-flame mixing is critical to NO_x formation in the axial stage [21-23]. The liftoff is defined as the distance from the center of the jet to the onset of the CH* signal after the threshold is applied. Liftoff was tracked temporally by applying this method to each image, and a time-averaged liftoff was determined by applying this method to the time-averaged flame taken from 20,000 images. The main sources of uncertainty for the liftoff are from the signal to noise ratio and pixel resolution. The signal to noise ratio was optimized for the

Table 1: Testing conditions. FP refers to the fully premixed configuration and NP refers to the non-premixed configuration. Each line of the fully premixed corresponds to three test conditions at three jet temperatures

Main Stage		Secondary Stage					Outlet		
T (°C)	v (m/s)	ϕ_{jet}	T_{jet} (°C) (Run 1; Run 2; Run 3)	J	v_{jet} (m/s) (Run 1; Run 2; Run 3)	Premix level	ΔT	T (°C)	CO (ppmVol)
1580	49	2.2	25; 150; 300	7.5	54; 64; 76	FP	220	1800	11; 12; 4
1650	51	2.1	25; 150; 300	5	45; 51; 62	FP	150	1800	14; 12; 5
1580	49	1.8	25; 150; 300	7.5	55; 65; 75	FP	170	1750	6; 6; 5
1650	51	1.5	25; 150; 300	5	46; 54; 63	FP	100	1750	11; 4; 16
1600	55	1.8	25; 150; 300	3.5	44; 53; 57	FP	50	1650	12; 14; 16
1580	49	2.2	300	7.5	76	NP	220	1800	10.3
1650	51	2.1	300	5	62	NP	150	1800	8.8
1580	49	1.8	300	7.5	75	NP	170	1750	11.0
1650	51	1.5	300	5	63	NP	100	1750	11.5

experiment, and a high-quality CH* filter was used that allows over 90% transmissibility in the 430 nm range. The spatial resolution for the chemiluminescence was 174 µm/pixel; because the liftoff heights are two orders of magnitude greater than this, the uncertainty associated with liftoff is expected to be on the order of 100 μm or 0.008 D_j.

2.3 Test Matrix

Table 1 provides the test conditions for the current investigation. Three different combustor exit temperatures were explored: 1650°C, 1750°C, and 1800°C, to simulate gas turbine baseload conditions and temperatures beyond current operation that would increase current efficiency. The goal of the test matrix is to decouple the effects of jet preheat temperature by maintaining a constant main stage temperature, temperature rise across the axial stage, and combustor exit temperature. To do this, the percentage of fuel and air to the axial stage was varied accordingly. By varying the fuel and air split to the axial stage, and modulating the headend flow rates appropriately, the same momentum flux ratio (*J*), equivalence

ratio (Φ_{jet}), and temperature rise (ΔT) was accomplished for a given condition. Momentum flux ratio (J) is defined as:

$$J = \frac{\rho_{jet} v_{jet}^2}{\rho_{cf} v_{cf}^2} \quad (1)$$

The overall air split to the axial stage ranged from 5.0%-10.6% while the fuel split ranged from 13.0%-15.9%. These splits lead to equivalence ratios ranging from 1.5-2.2; these splits were chosen in coordination with industry partners to maintain a reasonable velocity/momentum flux ratio for the given geometry. Because the adiabatic flame temperature increases with increasing reactant temperature, the overall equivalence ratio of the combustor was decreased with increased axial jet reactant temperature. The non-premixed configuration was employed for each of the 300°C cases to explore the effects of delaying ignition through a coaxial jet injection method in the axial stage.

3. Results

3.1 Jet Preheat Temperature

A major challenge associated with gas turbine combustion is the simultaneous mitigation of CO and NO_x emissions. At baseload, where overall firing temperature is increased, CO is sufficiently oxidized to CO_2. Thus, low levels of CO at the combustor exit are a strong indicator of complete combustion. For the current investigation, initial testing of the facility was to determine the length of the outlet to ensure adequate burnout from CO to CO_2. Table 2 shows the CO measurements made at the exit of the facility for each case run. The CO level for each condition

is below 20 ppmVol at the exit, with a majority less than 10 ppmVol. The non-premixed CO measurements are also below 20 ppmVol signifying the axial residence time is sufficient to burnout both the fully premixed and non-premixed configurations. The burnout of CO to CO_2 is critical to ensure NO_x measurements made are not influenced by low temperatures associated with incomplete combustion.

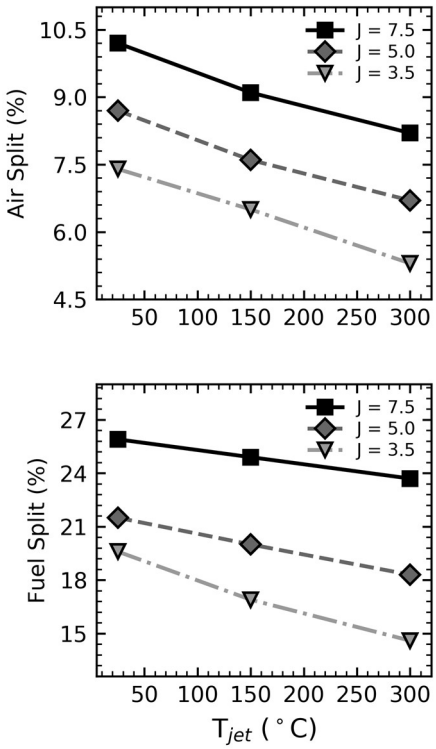

Fig. 5. Air and fuel split (by mass) for different jet temperatures required to maintain a constant momentum flux ratio, equivalence ratio, and temperature

To isolate the effects of jet temperature on NO_x emissions in the axial stage, the fuel and air split were varied to maintain a constant temperature rise at a fixed momentum flux ratio and equivalence ratio. Fig. 5 shows the fuel and air splits, by percent mass, for three different jet preheat temperatures. To isolate the effects of jet preheat temperature the fuel and air splits were adjusted to maintain a constant momentum flux (J), jet equivalence ratio (φ_{jet}), and temperature rise (ΔT). For each momentum flux ratio, both the fuel and air split to the axial stage decreases with increasing jet temperature due to the higher flame temperature from the preheated axial jet. For each constant momentum flux ratio line, the headend equivalence ratio and temperature were kept fixed; however, the headend conditions vary between different momentum flux ratios. To maintain a fixed temperature rise at a fixed outlet temperature, the total combustor equivalence ratio was varied slightly based on the axial jet temperature; for each case, the variation was around 3-5% based on the fuel and air split. Maintaining a constant

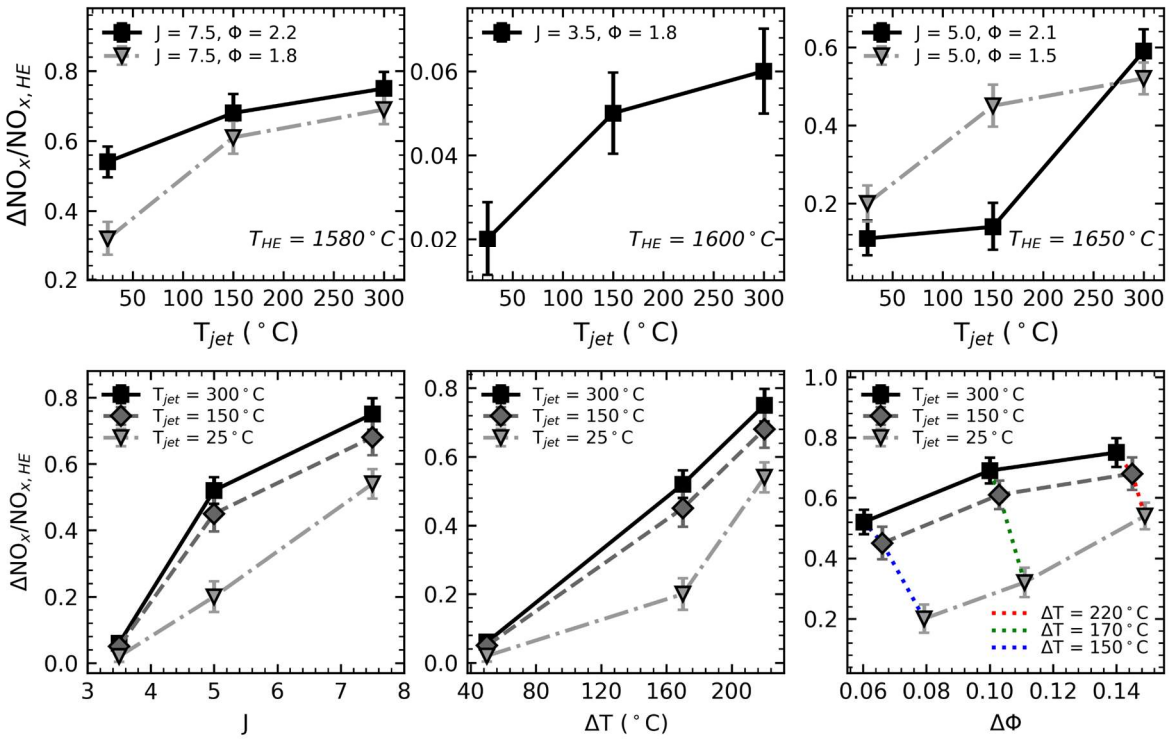

Fig. 6. NO_x measurements for varying preheat jet temperatures at various momentum flux ratios, temperature rises, and equivalence ratios increase. NO_x measurements are in ppmVol, corrected to 15% O2, and normalized by the headend NO_x.

temperature rise and firing temperature was chosen over a constant equivalence ratio rise and outlet equivalence ratio because temperature corresponds directly with efficiency in gas turbines.

NO_x measurements at the varying jet temperatures are presented in Fig. 6. The top row shows results at the three headend temperatures: 1580°C, 1600°C, and 1650°C plotted against the jet preheat temperature. For each fixed headend and exit temperature, an increase in jet temperature caused an increase in NO_x. NO_x formation for the 1600°C headend case was minimal due to the small temperature rise across the axial stage and decreased overall temperature output. While the temperature rise is fixed across the axial stage, the increase in equivalence ratio is not. For the increased jet temperature, the overall equivalence ratio of the combustor is slightly decreased to maintain a constant firing temperature. This leads to higher concentrations

of N_2 and O_2 which can dissociate and form NO; this is specifically important in the post flame gases where thermal NO forms via the thermal NO pathway [14].

To emphasize this trend, the bottom row of Fig. 6 shows the NO_x emissions as a function of momentum flux ratio, temperature rise, and equivalence ratio rise. For each parameter, the same trend is upheld, where increasing jet preheat temperature leads to elevated NO_x. Higher momentum flux ratios correspond to a greater fuel/air split to the axial stage which consequently leads to increased NO_x formation from the jet. For the axial stage temperature rise, a linear trend was seen for the three different jet preheat temperatures which consistent with previous research [21, 22]. The slope at which the NO_x emissions rise increases with increasing jet temperature, however. Initially, at a temperature rise of 50°C, the NO_x emissions for each jet preheat temperature closely match one another. As ΔT is increased, the NO_x levels between the jet temperatures diverge, and NOx formation is exacerbated at high ΔT and T_{jet}. The third plot in the bottom row shows NO_x emissions vs equivalence ratio rise. The red, green, and blue lines show the associated temperature rises for each condition; as mentioned previously, for a fixed temperature rise, the equivalence ratio increase will be higher for the lower jet temperatures to maintain a fixed combustor exit temperature. This is why the fixed ΔT lines are not vertical. At a fixed jet temperature, NO_x emissions increase linearly with equivalence ratio rise across the axial stage.

Fig. 6 depicted a strong correlation between NO_x emissions and preheat temperature. Previous research has shown a strong correlation between flame liftoff and NO_x emissions in the axial stage [21, 22]. For this reason, flame liftoff as a function of jet preheat temperature is now investigated. Flame liftoff is important for the axial jet as entrainment of additional crossflow

oxidizer prior to ignition can mitigate local regions that are near stoichiometric conditions mitigating NO formation within the flame. As a result, strategies to increase flame liftoff in the axial stage are critical to NO_x reduction. These effects are particularly prominent at elevated pressure where concentrations are higher and reaction rates are faster making pre-flame mixing between the jet and crossflow more challenging.

For each condition, the flame liftoff was assessed using CH* chemiluminescence imaging. Fig. 7 shows the time-averaged CH* chemiluminescence contours for each preheat temperature at J = 3.5, φ_{jet} = 1.8 jet (top row). The contours are normalized by the maximum intensity between the three time-averaged flames. The white lines in the figure show the liftoff distance from the center of the jet to the onset of the CH* signal. The stabilization point moves closer to the jet exit

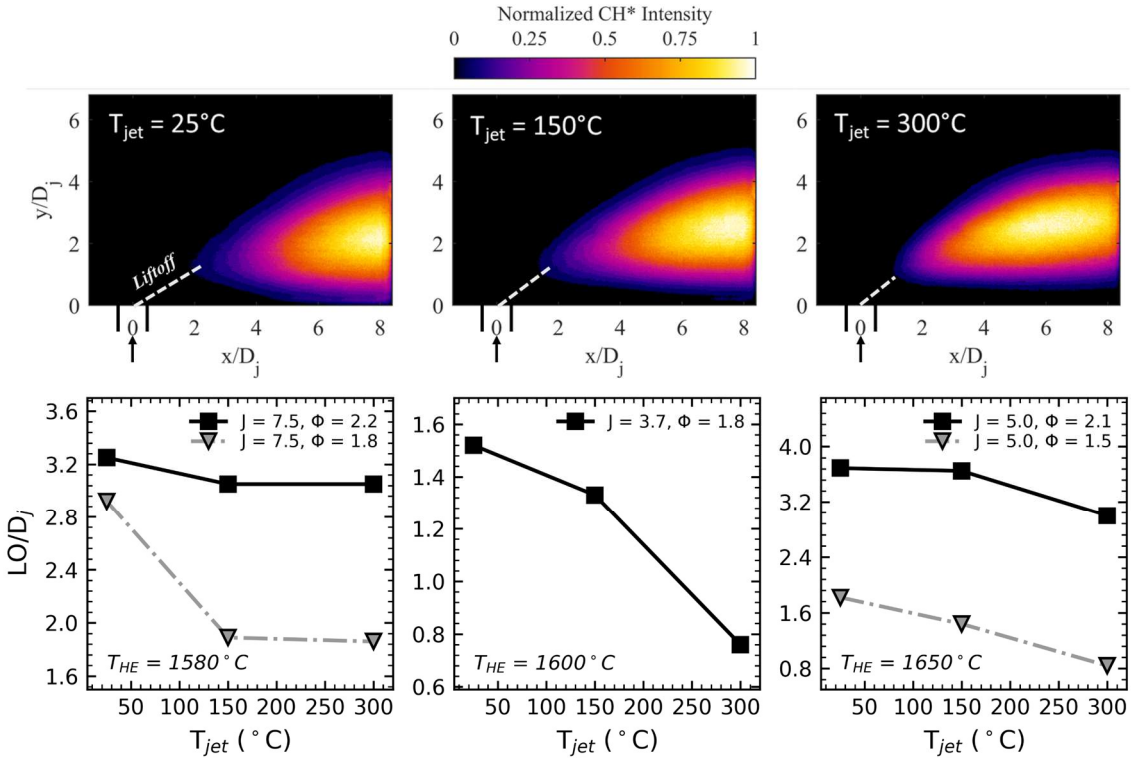

Fig. 7. Time-averaged CH* contours for J = 3.5, φ_{jet} = 1.8, at varying jet temperatures (top), and time-averaged liftoff for each condition at varying preheat temperature (bottom)

as the jet temperature is increased. Along with the stabilization point moving further upstream, the max CH* signal occurs further upstream as the jet preheat temperature is increased.

The time-averaged flame liftoff is presented in the bottom row of Fig. 7 for each condition. For reference, the liftoff distance is normalized by the 12.7 mm jet diameter. In general, increasing the jet temperature caused a decrease in liftoff; this effect was more pronounced in jets with equivalence ratios ranging from φ_{jet} = 1.5-1.8 compared to the richer equivalence ratios (φ_{jet} = 2.1-2.2). For each condition, an increase in equivalence ratio led to a more lifted flame. For the richer jets, additional oxidizer from the crossflow is required to mix with the jet to reach an ignitable mixture fraction. This inevitably causes an increase in flame liftoff.

The overall effects of temperature on liftoff are in agreement with Kolb et al. who investigated a similar phenomenon but at lower Reynolds numbers. At momentum flux ratios above 60, a similar trend between preheat temperature and liftoff was observed as in the current work. For momentum flux ratios 60 and below, the previous study did not observe any effects of preheat temperature on liftoff [20]. For the J = 6 condition, Kolb et al. reported a flame that was attached to the jet exit. For the current experiment, lifted flames are observed for each condition where momentum flux ratios range from 3.5-7.5. This suggests the effects of preheat temperature on flame liftoff are more dependent on velocity/Reynolds number than momentum flux ratio. This is likely an effect of higher Reynolds numbers in the current investigation, which leads to a more turbulent flow field where stabilizing a flame is more challenging.

The liftoff point is associated with the timescale required for the flame to ignite. An ignition timescale, τ_{ign}, has been used in previous research to understand the ignition delay in the axial stage, and is defined as follows [29]:

$$\tau_{ign} = \frac{LO}{v_{jet}} \quad (2)$$

Fig. 7 demonstrates that increasing jet temperature decreases flame liftoff. In addition, increasing the jet temperature proportionately decreases the jet density. To maintain a constant momentum flux ratio as the jet temperature is increased, the jet velocity must be increased to offset the decrease in density. The increase in jet velocity and decrease in liftoff will decrease the ignition timescale with increasing temperature. The remaining analysis will focus on the ignition timescale because it is more generalizable across conditions, accounts for flow dynamics, and is not as configuration dependent as flame liftoff.

The effects of jet preheat temperature on the ignition timescale is presented in Fig. 8; the top row shows the ignition timescale plotted against jet temperature. For each case, the ignition timescale decreases with jet temperature. This ignition timescale is indicative of how much time the jet reactants have to mix with the crossflow before ignition; for rich jets specifically, the entrainment of additional oxidizer prior to ignition is important to decrease the local equivalence ratio for prompt NO_x mitigation. The bottom row of Fig. 8 shows the NO_x measurements plotted against the ignition timescale. A strong trend is observed: as the ignition timescale is increased, the NO_x contribution of the axial stage decreases. This corresponds directly to decreasing the thermal delay generated by increasing the jet temperature. For the T_{jet} = 25°C, J = 7.5, and φ_{jet} = 1.8 condition (bottom left, grey dashed line), the ignition timescale is significantly higher than the 150°C and 300°C cases which results in substantially lower NO_x from the axial jet. Similarly,

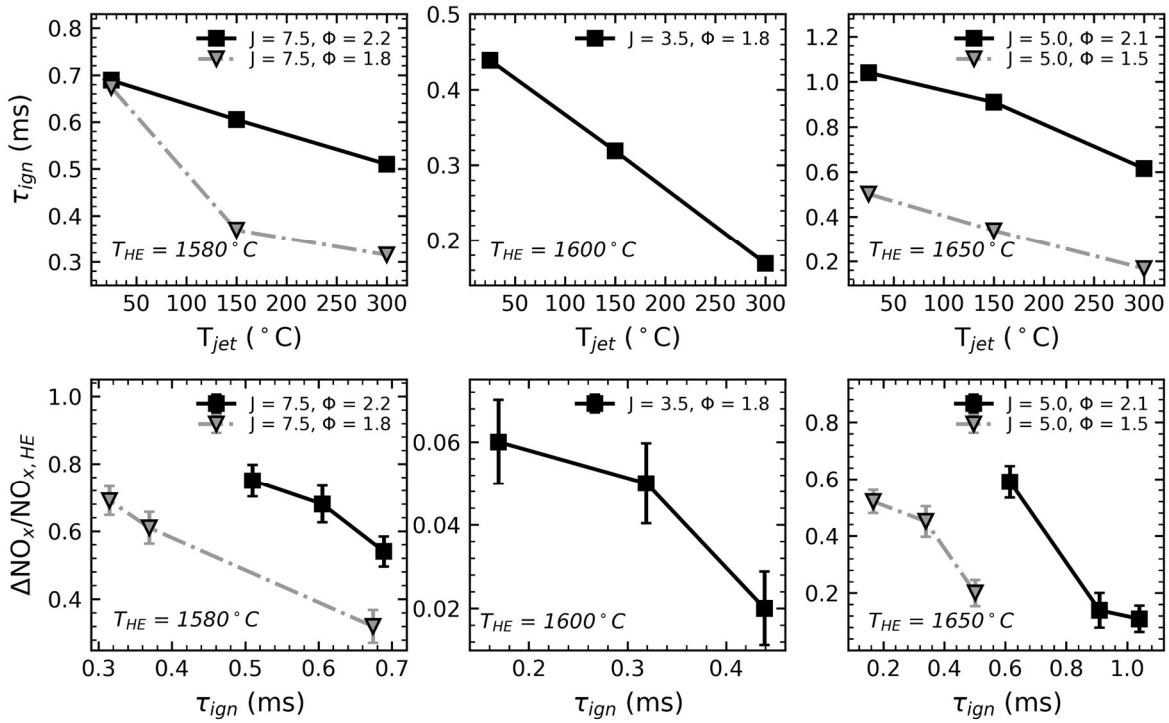

Fig. 8. Effects of preheat temperature on ignition timescale introduced in equation 2. Note: increasing velocity corresponds to increasing jet temperature (top row). Effect of ignition delay on NO_x emissions across axial stage (bottom row). NO_x measurements are in ppmVol, corrected to 15% O2, and normalized by the headend NO_x.

for the J = 5.0 and φ_{jet} = 2.1 condition (bottom right, solid black line), both the T_{jet} = 25°C and T_{jet} = 150°C have much higher ignition timescales compared to the 300°C case and have significantly lower NO_x levels.

In addition to having a strong effect on the ignition delay, varying the jet preheat temperature changes the flow-field. The density ratio (s) and velocity ratio (v_r) are important jet parameters that affect the mixing between the jet and crossflow. The density ratio is defined as the density of the jet divided by the density of the crossflow $s = (\rho_{jet}/\rho_{cf})$, while the velocity ratio is defined as the velocity of the jet divided by the velocity of the crossflow $v_r = (v_{jet}/v_{cf})$. These two parameters are related to the momentum flux ratios by:

$$J = sv_r^2 \tag{3}$$

An increase in either the density ratio or velocity ratio enhances mixing between two different fluid streams [36-38]. Increasing the jet temperature decreases the density ratio between the jet reactants and crossflow products; for the specific conditions run in this study, increasing jet temperature increases the velocity ratio between the jet reactants and crossflow products.

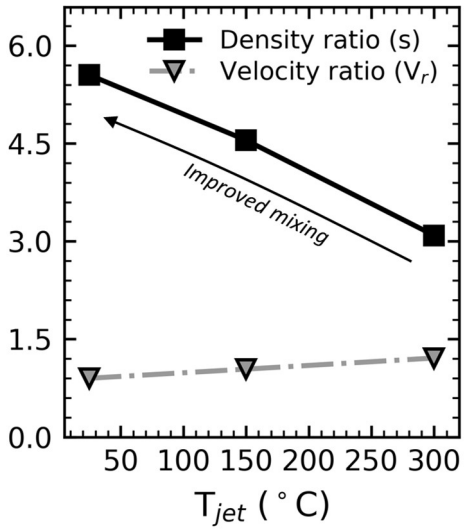

Fig. 9. Effects of preheating on density and velocity ratio for a constant J = 5.0

Fig. 9 shows the effects of jet temperature on the density and velocity ratio for the J = 5.0, φ = 1.5 condition. From the 25°C case to the 300°C case, the density ratio changes from 5.46 to 3.45 while the velocity ratio changes minimally from 0.95 to 1.25. The higher density ratio for the lower temperature jets leads to a stronger Rayleigh Taylor instability which ultimately leads to improved turbulent mixing. This suggests the lower temperature jets can mix better with the crossflow before ignition compared to the higher temperature jets. The results shown in Fig. 8 demonstrated an increase in ignition delay for the lower temperature jets; this coupled with the more favorable mixing configuration creates an advantageous condition for NO_x mitigation. Thus, a strong NO_x reduction is achieved by generating a thermal delay in the axial stage.

3.2 Non-Premixed Configuration and Comparative Analysis

The analysis from the previous section indicates a strong correlation between ignition delay and NO_x emissions for premixed jets subjected to preheating effects. To further investigate the effects of liftoff and emissions, the non-premixed configuration introduced in section 2.1 and

visualized in Fig. 3 is employed for each of the 300°C cases at the same jet/headend composition and flow-field. This allows for a comparison between the thermal delay investigated in section 3.1 and the fluid delay that will be introduced in the current section. This coaxial jet injection introduces a new variable in the ignition process of the axial stage: the mixing between the jet fuel and air must reach an ignitable mixture fraction along with reaching the autoignition temperature. This configuration is similar to the co-flow jet flame investigated by Gore and Zhan who explored a methane fuel jet with coaxial air injected around it into quiescent air for equivalence ratios ranging from 1.3-10 [15]. However, there are a few key fundamental differences in the current configuration: the coaxial jet is being injected orthogonally into oxygen-depleted vitiated products that have a high velocity and temperature, and the ignition of the jet is driven by heat transfer from the hot crossflow products to the jet. In the jet and crossflow coaxially injected configuration, there are two different mixing fluid streams: the coaxially injected air and the center tube fuel, and the coaxially injected air and the crossflow products. These mixing streams are critical for emissions formation; by delaying ignition through a coaxial injection, additional hot oxidizer can entrain into the jet from the crossflow prior to ignition.

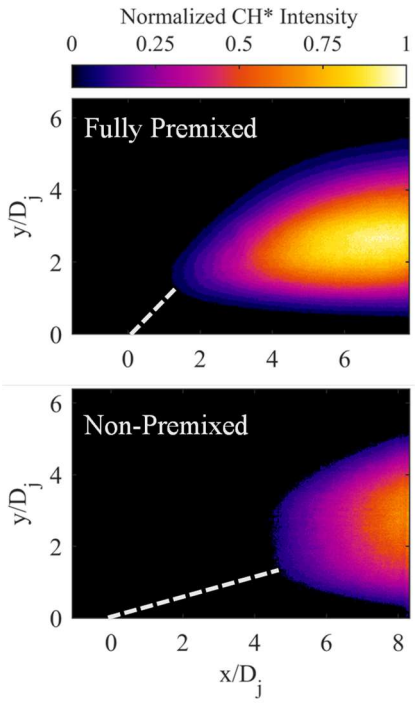

Fig. 10. Time-averaged, normalized false color CH* chemiluminescence contour for fully premixed (top) and non-premixed (bottom) for J = 7.5, φ_{jet} = 1.8 condition. Note: both jets are preheated to 300°C

Fig. 10 presents the time-averaged CH* chemiluminescence contour for the fully premixed and non-premixed J = 7.5, φ_{jet} = 1.8 condition. As expected, injecting the fuel and air

coaxially and forcing them to mix in the facility causes the flame to burn further downstream compared to the fully premixed condition. The max CH* signal for the fully premixed flame increases in the axial direction until x/D_j = 7.1 where it reaches its max intensity and then decreases to the end of the viewing window. For the non-premixed flame, the CH* signal increases in the axial direction reaching its maximum intensity at the end of the viewing window indicating a majority of the flame burns further downstream of the viewing window. Interestingly, despite the earlier ignition of the fully premixed jet, both flames penetrate similar distances in the y/D_j direction and span similar heights at the end of the viewing window.

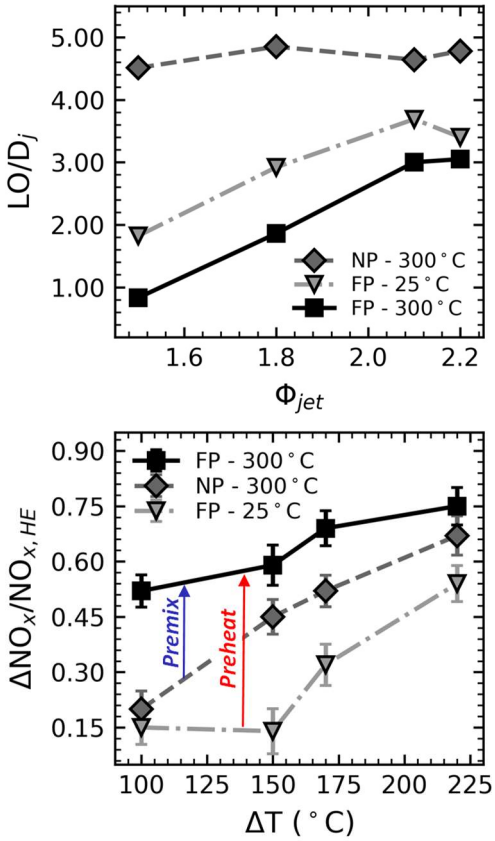

Fig. 11. Liftoff of the fully premixed 25°C and 300°C and non-premixed 300°C cases vs. Φ_{jet} (top) and NO_x measurements vs. temperature rise (ΔT) for the fully premixed 25°C and 300°C and non-premixed 300°C cases (bottom). NO_x measurements are in ppmVol, corrected to 15% O_2, and normalized by the headend NO_x.

As made evident by Fig. 10, the non-premixed configuration has a prominent effect on liftoff/ignition delay. The top chart of Fig. 11 shows the jet liftoff for the fully premixed 300°C and the non-premixed 300°C cases vs jet equivalence ratio. At φ_{jet} = 1.5, there is a large variation in liftoff between the fully premixed and non-premixed 300°C configurations. As the jet equivalence ratio is increased, however, this variation decreases. Similar to the jet preheat temperature, as the equivalence ratio is increased past an ignitable mixture, additional oxidizer from the crossflow is required to mix with the jet for the flame to ignite. Because of this, the effects of the

non-premixed configuration become suppressed with increasing equivalence ratio as the ignition of the fully premixed jet is no longer solely dependent on reaching the autoignition temperature. It is also observed that there is only a minor variation in liftoff over the range of equivalence ratios investigated for the non-premixed cases. This suggests the mixing between the coaxially injected fuel and air is the predominant factor in the ignition delay of the non-premixed configuration.

The bottom chart of Fig. 11 provides the NO_x emissions for the fully premixed 300°C and non-premixed 300°C cases vs axial stage temperature rise. Similar to the fully premixed jets from section 3.1, NO_x emissions increase linearly with increasing temperature rise for the non-premixed condition. This increase temperature rise is accompanied by higher equivalence ratios and momentum flux ratios. As this temperature rise increases, the variation in NO_x between the fully premixed and non-premixed conditions decrease. This is coupled to the decreased difference in liftoff between the two configurations as the jet equivalence ratio is increased as shown in the top chart of Fig. 11. These results agree with Sirignano et al. who investigated rich axial jets in an atmospheric facility over a range of equivalence ratios (φ_{jet} = 1-9) and momentum flux ratios (J = 1-4) [21, 22]. Varying φ_{jet} and J altered the flame liftoff, and ultimately NO_x emissions. It was found that for a fixed $\Delta\varphi$, an increase in jet equivalence ratio led to an increase in liftoff which ultimately provided a reduction in NO_x. At equivalence ratios above 3.4 however, NO_x emissions were found to increase again. In the current study, for the non-premixed configuration, the jet and headend compositions and flow-fields are fixed and the injection method in the axial stage is changed to vary the ignition delay. Despite this, similar results are seen concerning the effects of increasing jet equivalence ratio on the formation of NO_x from the

axial stage where increasing liftoff creates a NO_x reduction, but at higher jet equivalence ratios this benefit is not as strong.

The preceding analysis demonstrated NO_x reduction through ignition delay by two different methods: preheating and premixing. Plotted in Fig. 11 are NO_x measurements for the fully premixed and non-premixed 300°C jet with the addition of the fully premixed 25°C to compare the two ignition delay mechanisms. For each configuration, an increase in temperature rise across the axial stage leads to an increase in NOx emission from the axial jet. More notably, the NO_x reduction generated through a thermal delay overshadows the benefit of the premixing delay. In either case, the change in NO_x emissions is linked to pre-flame mixing and the entrainment of oxidizer into the axial jet. However, the physical mechanism that drives entrainment and mixing is different between preheating and premixing effects. As previously discussed, lower axial jet temperatures will drive a higher density ratio and thus provide a more favorable condition for mixing. In contrast, switching from a premixed to a non-premixed configuration induces mixing between fluid streams within the jet. Because the fuel and air are not premixed before injection, the non-premixed configuration could still have local hot spots caused by poorly mixed regions. Based on the data in Fig. 11, it is expected that the mixing environment provided by low-temperature jets affords improved entrainment characteristics compared to the non-premixed configuration, thus minimizing NO_x emissions.

4. Conclusion

NO_x emissions measurements of rich methane-air reacting jets in crossflows were presented over a range of industry-relevant conditions at an elevated pressure of 5 atm. The

effects of jet preheat temperature was investigated by fixing the momentum flux ratio, jet equivalence ratio, and temperature rise across the axial stage and varying the jet temperature from 25-300°C. Over the range of conditions explored, decreasing jet temperature led to a decrease in NO_x emissions observed in the axial stage. Fixing the momentum flux ratio and varying the jet temperature had a more substantial effect on the density ratio compared to the velocity ratio. For the velocities run in the current experiment, decreasing jet temperature led to a small decrease in velocity ratio, while the density ratio increased considerably. The higher density ratios at lower jet temperatures create a favorable environment for pre-flame mixing. This, along with the increase in ignition delay, was determined to be the cause of the lower NO_x levels at the lower jet temperatures.

A non-premixed coaxial injector was also studied at the same conditions as the fully premixed jet. The configuration was run for each 300°C case and provided a NO_x reduction compared to the fully premixed 300°C jets. The coaxial injection method pushed the flame further downstream compared to the fully premixed configuration allowing additional hot crossflow oxidizer to mix with the jet before ignition. The NO_x benefit of the coaxial injector was observed to decrease with increasing equivalence ratio as the ignition delay for the fully premixed and non-premixed configuration began to converge.

Amongst the cases explored, the effects of preheating and premixing were compared to one another. Ultimately, the NO_x emissions were more sensitive to preheating effects than premixing effects. In general, both methods of NO_x reduction rely on elongating the flame's ignition delay time. However, the results demonstrate that a temperature (or heat transfer) driven delay is more beneficial to NO_x mitigation than a fluid mechanical delay that relies more

heavily on mixing. Additionally, the elongated ignition delay is typically linked with larger flame liftoff. However, the results demonstrate that increased flame liftoff is not necessarily directly correlated with reduced emissions. For instance, a heated non-premixed jet was shown to have a larger liftoff than an ambient temperature premixed jet, yet the premixed ambient jet provided smaller NO_x. This suggests that the link between ignition delay (or flame liftoff) and emissions is also dependent on the physical mechanisms that drive the delay. Classical descriptions of premixed and non-premixed flames suggest NO_x emissions will be larger for non-premixed configurations due to local hot spots. For axial stage combustion, non-premixed jets allow more time for pre-flame mixing between the jet and crossflow which was shown to reduce NO_x. However, for the non-premixed jet, it is expected local hot regions are the source of increased NO_x emissions compared to the non-preheated axial jet. Additionally, the non-preheated jet creates a favorable flow-field for enhanced entrainment compared to the preheated non-premixed jet. However, high-fidelity spatiotemporal measurements or simulations would be required to validate or confirm these hypotheses. Ultimately, creating the largest ignition delay and most favorable flow-field environment for entrainment leads to the greatest NO_x reduction. These results provide a road map for NO_x mitigation for both current and future power generating gas turbines. Specifically, for the transition to carbon-free fuels such as hydrogen, these techniques are highly applicable.

References

[1] L.B. Davis, Dry Low NOx Combustion Systems for GE Heavy-Duty Gas Turbines, ASME Turbo-Expo (1996), paper 96-GT-027.
[2] K.M. Düsing, A. Ciani, U. Benz, A. Eroglu, K. Knapp, Development of GT24 and GT26 (Upgrades 2011) Reheat Combustors, Achieving Reduced Emissions and Increased Fuel Flexibility, ASME Turbo-Expo (2013), paper GT2013-95437.
[3] G. Myers, D. Tegel, M. Feigl, F. Setzer, W. Bechtel, D. Fitts, B. Couture, R. Tuthill, Dry, Low Emissions for the 'H' Heavy-Duty Industrial Gas Turbines: Full-Scale Combustion System Rig Test Results, ASME Turbo-Expo (2003), paper GT2003-38193.
[4] C.L. Vandervort, 9 ppm NOx/CO Combustion System for "F" Class Industrial Gas Turbines, J. Eng. Gas Turbine Power 123 (2001) 317-321.
[5] W.D. York, B.W. Romig, M.J. Hughes, D.W. Simons, J.V. Citeno, Premixed Pilot Flames for Improved Emissions and Flexibility in a Heavy Duty Gas Turbine Combustion System, ASME Turbo-Expo (2015), paper GT2015-44102.
[6] C.T. Bowman, Control of combustion-generated nitrogen oxide emissions: Technology driven by regulation, Symp. (Int.) Combust. 24 (1992) 859-878.
[7] J. Wagner, S. Grib, J. Dayton, M. Renfro, B. Cetegen, Flame stabilization analysis of a premixed reacting jet in vitiated crossflow, Proc. Combust. Inst. 36 (2016).
[8] J.A. Wagner, S.W. Grib, M.W. Renfro, B.M. Cetegen, Flowfield measurements and flame stabilization of a premixed reacting jet in vitiated crossflow, Combust. Flame 162 (2015) 3711-3727.
[9] J.W. Dayton, K. Linevitch, B.M. Cetegen, Ignition and flame stabilization of a premixed reacting jet in vitiated crossflow, Proc. Combust. Inst. 37 (2019) 2417-2424.
[10] M.D. Pinchak, V.G. Shaw, E.J. Gutmark, The effects of nozzle geometry and equivalence ratio on a premixed reacting jet in vitiated cross-flow, Combust. Flame 191 (2018) 353-367.
[11] M.D. Pinchak, V.G. Shaw, E.J. Gutmark, Flow-field dynamics of the non-reacting and reacting jet in a vitiated cross-flow, Proc. Combust. Inst. 37 (2019) 5163-5171.
[12] M.D. Pinchak, V.G. Shaw, E.J. Gutmark, The effects of cross-flow fuel injection on the reacting jet in vitiated cross-flow, Combust. Flame 199 (2019) 352-364.
[13] Z. Li, Y. Yuan, B. Guo, V.L. Varsegov, J. Yao, The Recirculation Zone Characteristics of the Circular Transverse Jet in Crossflow, Energies 13 (2020).
[14] K. Kuo, Principles of Combustion, John Wiley & Sons, New Jersey, 2005, pp. 255-262.
[15] J.P. Gore, N.J. Zhan, NOx emission and major species concentrations in partially premixed laminar methane/air co-flow jet flames, Combust. Flame 105 (1996) 414-427.
[16] K.H. Lyle, L.K. Tseng, J.P. Gore, N.M. Laurendeau, A study of pollutant emission characteristics of partially premixed turbulent jet flames, Combust. Flame 116 (1999) 627-639.
[17] T.K. Kim, B.J. Alder, N.M. Laurendeau, J.P. Gore, Exhaust and In-Situ Measurements of Nitric Oxide for Laminar Partially Premixed C2H6-Air Flames: Effect of Premixing Level at Constant Fuel Flowrate, Combust. Sci. Technol. 110-111 (1995) 361-378.
[18] J.F. Driscoll, R.-H. Chen, Y. Yoon, Nitric oxide levels of turbulent jet diffusion flames: Effects of residence time and damkohler number, Combust. Flame 88 (1992) 37-49.
[19] S.R. Turns, F.H. Myhr, R.V. Bandaru, E.R. Maund, Oxides of nitrogen emissions from turbulent jet flames: Part II—Fuel dilution and partial premixing effects, Combust. Flame 93 (1993) 255-269.

[20] M. Kolb, D. Ahrens, C. Hirsch, T. Sattelmayer, A Model for Predicting the Lift-Off Height of Premixed Jets in Vitiated Cross Flow, J. Eng. Gas Turbine Power 138 (2016) 1-9.
[21] M.D. Sirignano, V. Nair, B. Emerson, J. Seitzman, T.C. Lieuwen, Nitrogen oxide emissions from rich premixed reacting jets in a vitiated crossflow, Proc. Combust. Inst. 37 (2019) 5393-5400.
[22] M.D. Sirignano, V. Nair, B.L. Emerson, J. Seitzman, T.C. Lieuwen, Nitrogen Oxide Emissions from Premixed Reacting Jets in a Vitiated Crossflow, Combust. Sci. Technol. 192 (2020) 1389-1419.
[23] D. Ahrens, M. Kolb, C. Hirsch, T. Sattelmayer, NOx Formation in a Reacting Premixed Jet in Hot Cross Flow, ASME Turbo-Expo (2014), paper GT2014-26139.
[24] E. Goh, M. Sirignano, J. Li, V. Nair, B. Emerson, T. Lieuwen, J. Seitzman, Prediction of minimum achievable NOx levels for fuel-staged combustors, Combust. Flame 200 (2019) 276-285.
[25] P.P. Panda, O. Busari, R.P. Lucht, W.R. Laster, Effect of the nature of vitiated crossflow on the flow-field of a transverse reacting jet, Exp. Fluids 58 (2017) 1-16.
[26] P.P. Panda, O. Busari, M. Roa, R.P. Lucht, Flame stabilization mechanism in reacting jets in swirling vitiated crossflow, Combust. Flame 207 (2019) 302-313.
[27] P.P. Panda, M. Roa, C.D. Slabaugh, S. Peltier, C.D. Carter, W.R. Laster, R.P. Lucht, High-repetition-rate planar measurements in the wake of a reacting jet injected into a swirling vitiated crossflow, Combust. Flame 163 (2016) 241-257.
[28] P.P. Panda, M. Roa, P. Szedlacsek, W.R. Laster, R.P. Lucht, Structure and dynamics of the wake of a reacting jet injected into a swirling, vitiated crossflow in a staged combustion system, Exp. Fluids 56 (2015) 1-20.
[29] R. Sullivan, B. Wilde, D.R. Noble, J.M. Seitzman, T.C. Lieuwen, Time-averaged characteristics of a reacting fuel jet in vitiated cross-flow, Combust. Flame 161 (2014) 1792-1803.
[30] W.G. Lamont, M. Roa, S.E. Meyer, R.P. Lucht, Emission Measurements and CH* Chemiluminescence of a Staged Combustion Rig for Stationary Gas Turbine Applications, J. Eng. Gas Turbine Power 134 (2012) 1-7.
[31] M. Roa, W.G. Lamont, S.E. Meyer, P. Szedlacsek, R.P. Lucht, Emission Measurements and OH-PLIF of Reacting Hydrogen Jets in Vitiated Crossflow for Stationary Gas Turbines, ASME Turbo-Expo (2012), paper GT2012-68711.
[32] C. Prathap, F.C.C. Galeazzo, P. Kasabov, P. Habisreuther, N. Zarzalis, C. Beck, W. Krebs, B. Wegner, Analysis of NOX Formation in an Axially Staged Combustion System at Elevated Pressure Conditions, J. Eng. Gas Turbine Power 134 (2012) 1-8.
[33] N.S. Rodrigues, O. Busari, W.C.B. Senior, C.T. McDonald, Y. Chen, A.J. North, W.R. Laster, S.E. Meyer, R.P. Lucht, NOX reduction in an axially staged gas turbine model combustor through increase in the combustor exit Mach number, Combust. Flame 212 (2020) 282-294.
[34] T. Genova, M. Otero, J. Reyes, S. Martin, K.A. Ahmed, Partial Premixing Effects on the Reacting Jet of a High-Pressure Axially Staged Combustor, J. Eng. Gas Turbine Power 144 (2021) 1-6.
[35] N. Otsu, A Threshold Selection Method from Gray-Level Histograms, IEEE Trans. Syst. Man Cybern. Syst. 9 (1979) 62-66.
[36] G.L. Brown, A. Roshko, On density effects and large structure in turbulent mixing layers, J. Fluid Mech. 64 (1974) 775-816.
[37] P.E. Dimotakis, Turbulent Free Shear Layer Mixing and Combustion, Prog. Astronaut. Aeronaut. 137 (1991) 265-340.
[38] P.E. Dimotakis, Two-dimensional shear-layer entrainment, AIAA J. 24 (1986) 1791-1796.